A&A 482, 541–548 (2008)
DOI: 10.1051/0004-6361:20078964

Astronomy & Astrophysics

Chemical and morphological evolution of a silicate surface under low-energy ion irradiation

C. Davoisne[1,2], H. Leroux[1], M. Frère[2], J. Gimblot[2], L. Gengembre[2], Z. Djouadi[3], V. Ferreiro[1], L. d'Hendecourt[3], and A. Jones[3]

[1] Laboratoire de Structure et Propriétés de l'État Solide, UMR 8008, CNRS and Université des Sciences et Technologies de Lille, 59655 Villeneuve d'Ascq, France
e-mail: hugues.leroux@univ-lille1.fr
[2] Unité de Catalyse et de Chimie du Solide, UMR 8181, CNRS and Université des Sciences et Technologies de Lille, 59655 Villeneuve d'Ascq, France
[3] Institut d'Astrophysique Spatiale (IAS), UMR 8617, Université Paris-Sud 11 and CNRS, 91405 Orsay, France

Received 30 October 2007 / Accepted 23 January 2008

ABSTRACT

Aims. Olivine surfaces have been subjected to low-energy ion irradiation with H^+, He^+ and Ar^+ at energies within the keV range in order to simulate the effects of energetic gas-grain interactions within shocked regions of the interstellar medium.
Methods. The induced modifications in the chemical composition and the bonding configuration of the upper and the near surface regions were monitored in situ by X-ray photoelectron spectroscopy (XPS). The associated morphological evolution of the samples was studied by atomic force microscopy (AFM).
Results. Results show that the surface chemistry evolves during irradiation with a noticeable Mg enrichment relative to Si. This evolution is interpreted as coming from magnesium atom diffusion driven by the electric field caused by the positive ion implantation. The iron valence state is also strongly affected by irradiation, with reduction occurring at relatively high fluxes. However, at low fluxes the iron is found to oxidise from Fe^{2+} to Fe^{3+} due to a charge transfer between the incident positive ions and the iron in the sample. The atomic force microscopy results show that the surface roughness tends to increase with irradiation and that this roughness influences the surface chemical reactivity of the grains, as shown by the enhanced formation of carbonate on the surfaces when they are exposed to a CO_2 atmosphere. The implications for the evolution of interstellar dust include an enhanced dust catalytic activity. These effects would arise from modification under irradiation of the surface reactivity and an increase in the available grain surface area.

Key words. ISM: dust, extinction – ISM: cosmic rays – methods: laboratory

1. Introduction

Interstellar dust is primarily synthesised in the shells around evolved stars (asymptotic and red giant branch, AGB and RGB, stars and supernovae). The ISO SWS and LWS spectrometers detected the signatures of crystalline silicates formed around evolved stars (Waters et al. 1996; Jäger et al. 1998; Sylvester et al. 1999; Demyk et al. 2000; Molster et al. 2002a,b). The crystalline signatures are attributed to Mg-rich olivine (forsterite, Mg_2SiO_4), Mg-rich pyroxene (enstatite, $MgSiO_3$), diopside ($CaMgSi_2O_6$), metal oxides and water ice. Around these same objects the amorphous silicate is mainly of olivine-type with less than 10% of pyroxene-type composition (Demyk et al. 2000). Through the effects of the stellar winds the dust is injected into the interstellar medium (ISM) where it resides for a long time until its incorporation into molecular clouds, star forming regions and then into the accretion discs around young stars. For the dust in the ISM, the ISO spectra show no evidence for presence of crystalline dust and indicate that the silicates are amorphous. The upper limit for the crystalline silicate dust in this environment has been estimated to be around 2%, in comparison with 10–40% around evolved stars (Kemper et al. 2004, 2005).

The differences in composition and/or crystallinity appear to occur during the transport of dust through the ISM where it is subjected to processes which modify its composition, structure, porosity and size distribution. These modifications likely take place within supernova-generated shock waves in which the gas is preferentially accelerated with respect to the dust (Jones et al. 1994; Ellison et al. 1997). A major result of this differential acceleration is an irradiation of the dust by ions in the tens of eV to keV energy regime, which is particularly efficient for the sputtering and amorphisation of the dust components (Tielens et al. 1994; Jones et al. 1996; Jones 2000, 2004; Demyk et al. 2001; Carrez et al. 2002).

Earlier experimental studies investigated the effects of irradiation with low-energy (4–50 keV) ions (H^+, He^+, Ar^+) on the structure of olivine (Demyk et al. 2001, 2004; Carrez et al. 2002; Brucato et al. 2004), enstatite (Schrempel et al. 2002; Jäger et al. 2003; Demyk et al. 2004) and diopside (Demyk et al. 2004). These experiments showed that the structural modification results in the amorphisation of the sample as well as the formation of gas bubbles that result in a high porosity in the samples. Some studies also suggest that irradiation can also induce chemical changes, such as the preferential sputtering of particular atoms (magnesium and oxygen) from the silicate surface (Bradley 1994; Demyk et al. 2001; Carrez et al. 2002). Dukes et al. (1999) investigated the chemical modification of olivine during low-energy He^+ and H^+ irradiation (respectively, 4 keV and 1 keV) in a photoelectron spectrometer. They observed a

reduction of iron and a decrease in the oxygen concentration at the sample surface. These results suggest that the dust is severely modified (chemically and structurally) by the effects of ion irradiation in the ISM. However, these chemical modifications, all measured in irradiation experiments, do not help to explain the odd depletions of some elements in the ISM. For instance silicon is rather more easily released into the gas in the ISM than expected, suggesting a preferential removal from the dust (e.g. Jones 2000), in contradiction with the experimental results. These disparities show that we still need to understand more about the chemical evolution of silicates under low-energy ion irradiation conditions. Another aspect which has not yet been addressed concerns the morphological modification induced by irradiation. Since the grain surfaces are the sites of surface-driven chemistry and critical in the initial phases of gas accretion in dense regions, surface processing by ion irradiation could significantly influence the kinetic accretion rates and catalytic properties.

In this study we present experimental results on the chemical and morphological modification of silicate surfaces under low-energy ion irradiation. The samples were irradiated and analysed in situ in a photoelectron spectrometer in order to measure the chemical changes of the surfaces during the irradiation process. The irradiated samples were studied by atomic force microscopy to establish the surface morphology. Finally, we have tested the chemical reactivity of an irradiated sample by exposure to carbon dioxide in order to assess the effects of irradiation on the silicate surface reactivity.

2. Experiment

2.1. The starting silicate

The samples used for this study are natural olivine from San Carlos (Arizona, USA), which have a bulk composition of $Mg_{1.8}Fe_{0.2}SiO_4$. The olivine crystals were cut with a precision saw to obtain slices 1 mm thick with parallel faces. One face was polished with SiC paper (1200, 2400, 4000 grade) then with 1/4 μm diamond solution and cleaned with ethanol before being irradiated.

2.2. X-ray photoelectron spectroscopy

X-ray photoelectron spectroscopy (XPS) is an electron spectroscopic technique for determining the nature and chemical composition changes of the surfaces of materials. It gives information on the surface composition, oxidation state and local bonding environments. This analytical technique has already been used to study the irradiation-induced modification of minerals (e.g. Dukes et al. 1999; Carrez et al. 2002). Further details of this technique, as well as some examples of mineralogical applications, can be found in Hochella (1988).

The measurements were performed using a Vacuum Generators Escalab 220XL spectrometer working with a non-monochromatised Al Kα X-ray source ($h\nu$ = 1486.6 eV) and were carried out in the high vacuum (about 10^{-10} Torr) analysis chamber. During XPS analysis the sample surfaces are bombarded by photons (Al Kα) and the interaction between the X-ray photons and the sample atoms ejects electrons from a given atomic core or valence level. If sufficient energy is transferred to the electrons, they can escape the sample surface and are collected by an electron analyser and sorted according to their binding energy (BE) or kinetic energy (KE) ($h\nu$ = BE + KE + ϕ, where $h\nu$ is the incident photon energy and ϕ is the work function of the spectrometer). An XPS spectrum presents the number of emitted electrons as a function of their binding energy or their kinetic energy. The measured binding energies are characteristic of the target atom and its chemical environment. During measurement Auger electrons arising from de-excitation processes can be also emitted and detected. The obtained spectra give qualitative and quantitative chemical information about the sample surface atoms to a depth not exceeding 10 to 15 nm.

The XPS data were processed by means of the Eclipse Software (from VG Scientific) after a Shirley-type baseline removal (Shirley 1972). For each characteristic peak the number of photoelectrons is counted and the composition of the sample determined. The normalised areas were used to calculate the atomic ratios of the outer layers according to:

$$\text{Normalised area} = (\text{peak area})/(T(E) \times \lambda(E) \times \sigma). \quad (1)$$

Where $T(E)$ is the transmission function of the spectrometer and $\lambda(E)$ is the mean free path of the photoelectrons in the solid sample. For inorganic compounds $\lambda(E) \sim \text{KE}^{0.77}$ according to Wagner et al. (1980) and Tamuna et al. (1993). σ is the photoelectron cross-section for the investigated atomic core level (Scofield 1976). Since the mean free paths of the electrons are small (typically a few nm) the detected electrons originate close to the surface. The simultaneous observation of the Mg 1s and Mg 2p features is of special interest because, as can be seen in the spectra of Fig. 1, the Mg 1s and Mg 2p peaks have a large difference in their kinetic energies (KE $\approx$ 182.6 eV for Mg 1s and 1436.4 eV for Mg 2p). Therefore the information depth from the uppermost surface layers probed in the sample is not the same because it is connected to the electron mean free path $\lambda(E)$ in the silicate lattice.

Assuming that $\lambda(E) \sim \text{KE}^{0.77}$, the ratio of the electron mean free paths for these two peaks is:

$$\frac{\lambda\text{Mg 2p}}{\lambda\text{Mg 1s}} = \left[\frac{\text{KE(Mg 2p)}}{\text{KE(Mg 1s)}}\right]^{0.77} \approx 4.9. \quad (2)$$

For the detection of photoelectrons emitted normal to the plane of the sample (as is the case for the VG Escalab spectrometer) about 95% of the signal comes from a depth corresponding to three times the electron mean free path (Grimblot 1995), therefore, the integrated Mg 2p photoelectron peak probes a depth five times larger than that for the Mg 1s electrons. In other words, the Mg 1s signal is much more surface sensitive than the Mg 2p peak.

The binding energies of O 1s, Si 2p, Mg 1s, Mg 2p and Fe $2p_{3/2}$ core levels were systemically determined during the recording of the spectra (see Table 1). The peak position of each band, before irradiation, was calibrated using the C 1s binding energy at 285 eV, the carbon being present as contamination. The Si 2p binding energy is in this case 101.9 eV, a value that is in good agreement with the 101.8 eV obtained by Guittet et al. (2001) for the Si 2p band in the SiO_4^{2-} environment in $ZrSiO_4$. After irradiation the carbon contamination is removed and so the Si 2p at 101.9 eV is used as the internal reference for the study.

2.3. Sample irradiation

The He^+ ion irradiation was performed in situ in the photoelectron spectrometer using a Penning ion gun (VG-AG500) located in the preparation chamber of the spectrometer at an incidence angle of 90° relative to the plane of the sample. The transfer of the sample from the preparation chamber (10^{-7} Torr)

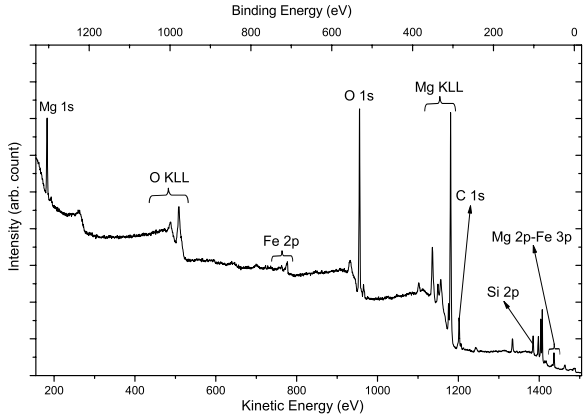

Fig. 1. Photoelectron spectrum of the San Carlos olivine before irradiation over a wide energy range. The peaks corresponding to C 1s, O 1s, Si 2p, Mg 1s, Mg 2p and Fe $2p_{3/2}$ core levels and the Auger structure (O KLL, Mg KLL) are indicated.

to the analysis chamber (10^{-10} Torr) was achieved under vacuum without exposure to air, thus avoiding contamination or oxidation of the samples. The samples were bombarded at 1 and 4 keV with He^+ ions at fluxes ranging from 3×10^{13} to 2×10^{15} ions cm^{-2} s^{-1} for various durations. The irradiated area of the sample was 6 mm diameter, adjusted to fit the dimension of the hole of the gold mask. The Ar^+ and H^+ ion irradiations were performed at 1 keV, with fluxes ranging from 3×10^{12} to 9×10^{12} ions cm^{-2} s^{-1}, in situ in the photoelectron spectrometer using an ion gun (VG-EX05). This ion beam was located in the analysis chamber of the spectrometer and was at an incident angle of 38° with respect to the samples. The chemical modification was measured by taking XPS spectra at regular intervals (ranging from 1 min to several hours). For a few samples, surface neutralization was performed after irradiation, using an electron flood gun in order to compensate for the electrostatic charge which can appear at the surface sample during irradiation. Before ion irradiation a gold mask with a 6 mm diameter hole in the center was placed on the samples in order to minimise charging effects and to limit the XPS analyzed area to that of the irradiated area.

2.4. Atomic force microscopy

The morphological surface modifications induced by irradiation in the photoelectron spectrometer were investigated using atomic force microscopy (AFM), a powerful tool for investigating surface morphology down to nm-size scales. The AFM observations were performed ex situ at room temperature, in air, using a Dimension 3100 microscope from Digital Instruments operating in the tapping mode. We used integrated silicon tips with tip radii of about 10 nm and cantilever spring constants of about 40 N/m. In this mode the cantilever oscillates vertically at a driven frequency that is close to its resonance frequency and contacts the sample surface briefly for each cycle of the oscillation. As the tip approaches the surface, the vibrational characteristics of the cantilever oscillation (e.g. amplitude, resonance frequency and phase angle) change due to the tip-sample interaction. Surface topography images were obtained by using the feedback loop which keeps the amplitude at a constant value (the set-point amplitude) by vertically translating the sample with the piezoelectric scanner. The recorded "height" images represent the topography of the surface. The AFM images were recorded with a high resolution, 512 × 512 pixels with a scan rate of 0.5 Hz. The surface roughness was measured using a Root Mean Square (rms) method.

Table 1. Electron binding energies for the olivine constituent atoms. The Si 2p band at 101.9 eV is used as a reference position.

Olivine constituent atoms	Binding energy (eV) (±0.2 eV) for the experimental samples
Si 2p	101.9
Mg 1s	1304.0
Mg 2p	50.2
O 1s	531.0–531.2
Fe^{3+} $2p_{3/2}$	711.6
Fe^{2+} $2p_{3/2}$	709.9
Fe^0 $2p_{3/2}$	706.3
C 1s (contamination)	285.0

3. Results

3.1. Chemical state of the samples before irradiation

Figure 1 shows a XPS spectrum over a wide energy range for a sample before irradiation. The binding energies were calculated using both the C 1s contaminant band at 285.0 eV and the intrinsic Si 2p level of olivine at 101.9 eV as references. Before irradiation the presence of carbon on the surfaces alters the determination of the surface composition. As a consequence, we opted for a thermal annealing of the sample under an O_2 atmosphere for 30 min at 500 °C in order to remove the C-rich contamination layer. The thermal treatment under O_2 was performed in the preparation chamber of the XPS and the samples were further analysed or irradiated without exposure to air. After this process the O 1s/Si 2p, Mg 1s/Si 2p, Mg 2p/Si 2p and Fe 2p/Si 2p ratios were found to be close to the theoretical ratios for olivine. The lattice oxygen O 1s and magnesium Mg 1s binding energies are located at 531.2 and 1304.0 eV respectively, in agreement with previous measurements obtained on olivine (Seyama & Soma 1985). Table 1 summarises the electron binding energies for all elements.

The shape of the Fe $2p_{1/2}$-Fe $2p_{3/2}$ doublet is complex due to satellite structures and multiplet effects due to paramagnetic species. The position of the maximum of the Fe $2p_{3/2}$ peak is sensitive to the iron valence state and is located, respectively, at 711.2 for Fe^{3+}, 709.8 for Fe^{2+} and at 706.8 eV for Fe^0 (Graat & Somers 1996). The proportions of the different iron oxidation states, in a given sample, can be determined by means of a Non Linear Least Square Fitting (NLLSF Eclipse Software from VG) approach. This software uses the reference spectra of the different iron states to fit the analysed spectrum and to determine the area corresponding to each state. The reference spectra used for this study were obtained using a stainless steel cleaned by Ar^+ irradiation for Fe^0, a thin film of $LiFePO_4$ for Fe^{2+} and a stainless steel oxidised in $HClO_4$ for Fe^{3+} (see Fig. 2). In the starting San Carlos olivine iron is predominantly in the Fe^{2+} state, in agreement with native olivine. However, we detected a small proportion of Fe^{3+}. The presence of Fe^{3+} at the sample surface is frequent, as mentioned by Schott & Berner (1983) and Dukes et al. (1999) for natural olivine samples.

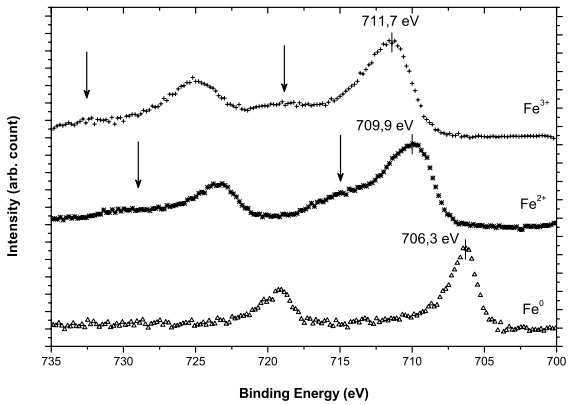

Fig. 2. Characteristic Fe 2p spectra of the three iron oxidation states. The peaks between 706 and 712 eV are due to Fe $2p_{3/2}$ and those between 717 and 725 eV correspond to Fe $2p_{1/2}$. The satellite peaks, which are characteristic of Fe^{2+} (small shoulder on the left of the main peak) and Fe^{3+} (bump in the middle of the two main peaks), are indicated by arrows. These features are used in the Non Linear Least Square Fit method to extract the relative proportion of each valence species of olivine.

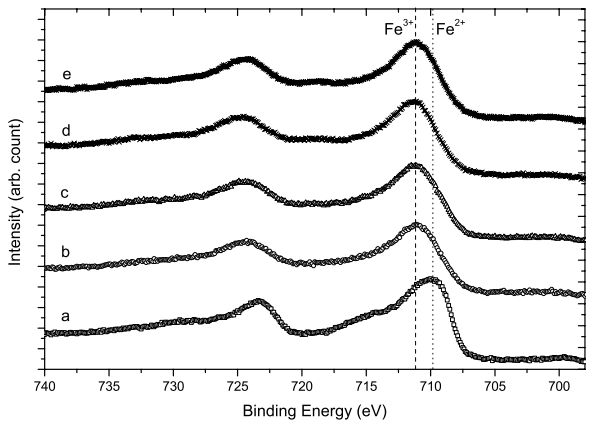

Fig. 3. XPS spectra of the Fe 2p region showing the progressive transformation of Fe^{2+} to Fe^{3+} during irradiation with He^+ at 4 keV and a flux of 4×10^{14} ions cm^{-2} s^{-1}: **a)** spectrum before irradiation, Fe^{2+} is the major valence state present at the olivine surface (85% of the iron), **b)** after irradiation with a fluence of 4×10^{17} He^+ cm^{-2}, **c)** with a fluence of 14×10^{17} He^+ cm^{-2}, the native oxide is progressively transformed to Fe^{3+} (38% of the iron in the Fe^{2+} state), **d)** after a fluence of 21×10^{17} He^+ cm^{-2} and **e)** a fluence of 29×10^{17} He^+ cm^{-2}, Fe^{3+} is the dominant valence state present in the sample surface (12.7% and 23.3% of the iron in the Fe^{2+} state for the respective fluences). The Fe $2p_{3/2}$ peak has moved from a binding energy of 710.3 eV to a binding energy of 711.7 eV after a fluence of 2.9×10^{18} He^+ cm^{-2}.

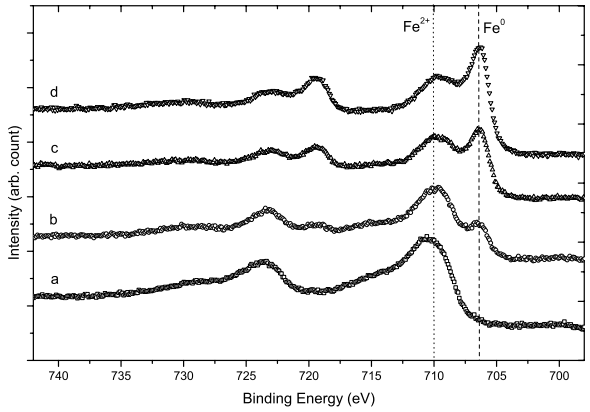

Fig. 4. Detail XPS spectra of the Fe 2p region showing a reduction of the iron species. The sample was irradiated with He^+ at 4 keV and 1.1×10^{15} ion cm^{-2} s^{-1}. A progressive reduction of the iron is indicated by the formation and development of the peak characteristic of the Fe^0 state at 706.3 eV and a decrease of the Fe^{2+} peak: **a)** before the irradiation, Fe^{2+} is the dominant state present, **b)** 6.7×10^{17} He^+ cm^{-2}, **c)** 23×10^{17} He^+ cm^{-2} and **d)** 38.6×10^{17} He^+ cm^{-2}.

3.2. Chemical state of the samples after irradiation

3.2.1. Evolution of peak position and shape

The peak positions are modified by irradiation, an effect that is mainly due to implantation into the samples and thus to a polarisation of the surface because olivine is an insulator. This charging effect is also partly due to the photoemission process during the recording of the XPS spectra. Electrical charging of the surface modifies the photoelectron kinetic energies and hence the measured binding energies of the representative core levels. All the peaks are found to be displaced towards lower binding energies with the same amplitude. In order to compare the peak positions, the Si 2p core level at 101.9 eV (BE) was chosen as an internal reference. The amplitude of the shift is found to increase progressively during irradiation but the relative positions of the peaks remain unchanged. It is to be noted also that the gold doublet at 88.0 and 84.0 eV from the Au $4f_{5/2}$ and Au $4f_{7/2}$ peaks, respectively, closely resembles the one of the non-irradiated area, suggesting that no gold was deposited on the surface due to sputtering. Indeed if gold is present on the irradiated surface as nanoparticles the doublet should have shown a shift as for other elements as a results of surface charging.

The Mg 1s, Mg 2p, O 1s and Si 2p peaks display an increase in full width at half maximum (FWHM) of about 0.4 eV. A possible explanation for this peak broadening is the development of structural disorder in the sample under ion irradiation, as seen in previous experiments with SiO_2 (Torrisi et al. 1996). This result is in agreement with the amorphisation of crystalline silicates observed under low-energy ion irradiation (Demyk et al. 2001, 2004; Carrez et al. 2002; Schrempel et al. 2002; Jäger et al. 2003; Brucato et al. 2004). The Mg Auger emission peak is not modified, indicating that the local chemical environment of the magnesium species is unchanged during irradiation.

3.2.2. Evolution of the iron oxidation state

The Fe 2p peak is strongly modified under irradiation and we find that the nature of the modification depends upon the incident ions and the fluxes. Fe oxidation has been observed with He^+ irradiation (1 and 4 keV) for fluxes below $\sim 6 \times 10^{14}$ ions cm^{-2} s^{-1} and with H^+ irradiation whatever the flux. This transformation is indicated by the formation of peaks at higher binding energies and the modification of the satellite peak structure, which are compatible with a progressive transformation from Fe^{2+} to Fe^{3+} (Fig. 3). The percentage of the Fe^{3+} state typically increased from 15% (before irradiation) to 80% after irradiation (for fluences of the order of 3×10^{18} ions cm^{-2}).

For Ar^+ (1 keV, all fluxes) and He^+ (1–4 keV, fluxes $>6 \times 10^{14}$ ions cm^{-2} s^{-1}), the iron species were reduced as indicated by the formation of peaks on the lower energy sides of the initial Fe $2p_{3/2}$ peak that is attributed to Fe^0 species. The initial Fe $2p_{3/2}$, characteristic of Fe^{2+} species, progressively decreases. Figure 4 illustrates this evolution for an irradiation experiment performed with He^+ at 4 keV.

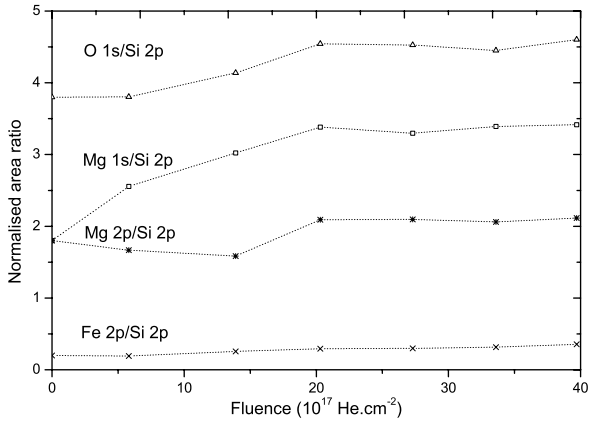

Fig. 5. Evolution of the normalised area ratio, relative to Si 2p, as a function of the fluence. The olivine sample was irradiated by He^+ at 4 keV (normal incidence) and with a flux of 4×10^{14} ions cm^{-2} s^{-1}. The main observed effect is an increase in the Mg 1s/Si 2p ratio, which is associated with magnesium segregation at the surface.

3.2.3. Evolution of the surface composition

The surface compositions were measured using the normalised area ratios with Si 2p as an internal reference. The ratios Mg 1s/Si 2p, Mg 2p/Si 2p and O 1s/Si 2p were found to increase while the Fe 2p/Si 2p ratios remained constant. The major observed change is the increase of Mg 1s/Si 2p ratio which evolves from 1.8 at low fluence to a maximum value of 3 at high fluences. Figure 5 shows the evolution of these ratios for a He^+ irradiation experiment. The other experiments display similar trends whatever the irradiation conditions (fluxes, energies or nature of the incident ion). The difference between the Mg 1s/Si 2p and the Mg 2p/Si 2p ratios is characteristic of a difference in the magnesium depth distribution in the sample. The Mg 1s photoelectrons come from a depth of approximately 1 nm whereas the Mg 2p photoelectrons come from a depth of approximately 5 nm. This differential evolution indicates a chemical change in the surface layers under the effects of ion irradiation, which tend to be enriched in MgO species.

3.3. Morphological surface change during irradiation

AFM measurements were performed before and after the irradiation experiments in order to image the morphological changes of the sample surfaces. The AFM images of the olivine sample before irradiation show straight stripes randomly distributed and with a mean depth of 6 nm for the majority of the stripes and a depth of 12 nm for the deeper ones (Fig. 6a). The stripes are a result of the mechanical polishing process during sample preparation.

After He^+ irradiation (4 keV, fluxes of 3×10^{14} to 1.1×10^{15} ions cm^{-2} s^{-1}) the polishing stripes are no longer apparent (Figs. 6b, c). The microstructure consists of hillock-like domains which rapidly developed with irradiation and are typically 50 nm in size (Fig. 6b). These domains are found to become progressively elongated with increasing the distance from the irradiation center (Fig. 6c). The domain elongation is oriented towards the center of the irradiated area. In comparison with the surface before irradiation, the sample roughness after He^+ irradiation had increased by a factor of 2, from 1.5 nm before irradiation to 3 nm after irradiation (Fig. 7). At 1 keV and for similar fluences, the domain size is found to be smaller, typically 20 nm size. An elongation is also observed at the periphery of the irradiated area (Fig. 6d).

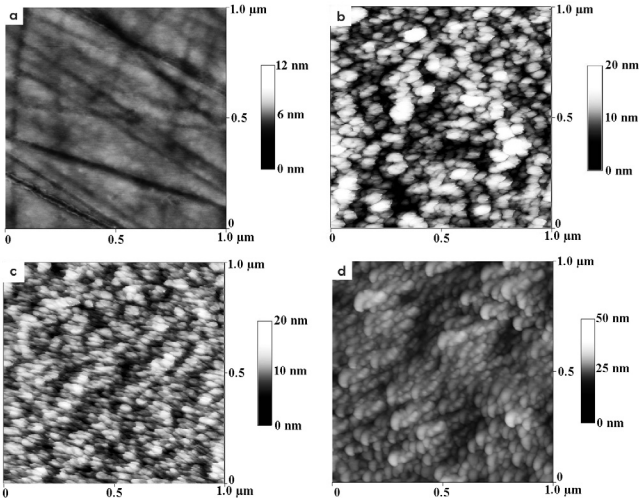

Fig. 6. AFM images: **a)** before irradiation, **b)** in the center of the irradiated area after He^+ irradiation (4 keV, fluence 1.1×10^{19} ions cm^{-2}), **c)** on the periphery of the irradiated area after He^+ irradiation (4 keV, fluence 1.1×10^{19} ions cm^{-2}) and **d)** after He^+ irradiation (1 keV, fluence 4.8×10^{18} ions cm^{-2}).

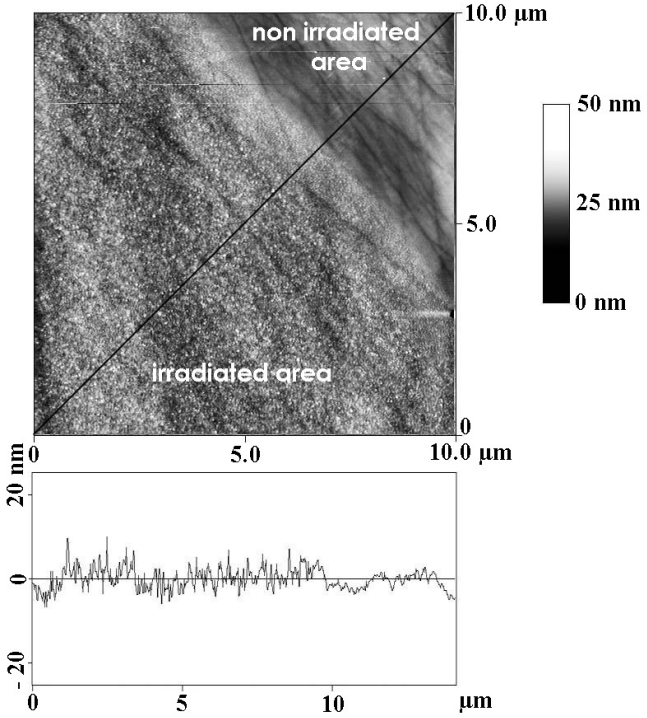

Fig. 7. AFM image (*top*) and roughness profile across the interface along the black line (*bottom*). The roughness of the irradiated area has increased by a factor of two.

After Ar^+ irradiation (1 keV, at normal incidence and flux 9×10^{12} ions cm^{-2} s^{-1}) the depth of the polishing grooves decreases to a mean depth of 3 nm. The main characteristic here is the formation of large hillocks on the surface, typically 180 nm in diameter and 20 nm in height (Fig. 8a). These hillocks are not stable with time. For instance, after one week of air exposure both their size and height decrease (Fig. 8b), suggesting a high reactivity of the irradiated surface.

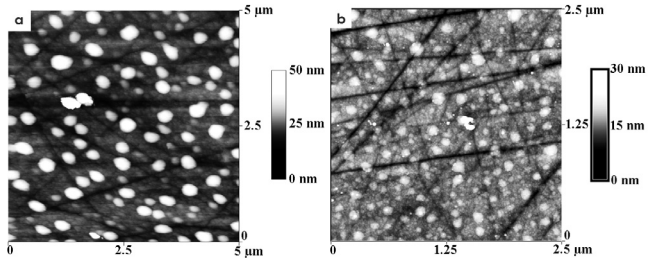

Fig. 8. AFM image of the olivine surface irradiated with Ar^+, at 1 keV and a fluence of 3.6×10^{16} ions cm^{-2}: **a)** just after irradiation and **b)** after one week of exposure to air.

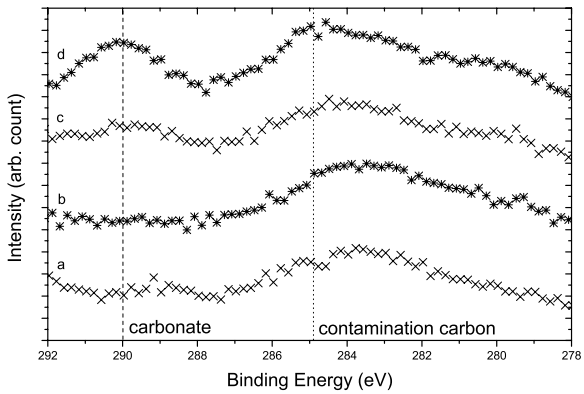

Fig. 9. XPS spectra of the C 1s region: **a)** after thermal annealing under an O_2 atmosphere, a weak carbon contamination band at a binding energy of. 285 eV is still present (dotted line), **b)** after thermal annealing under O_2 atmosphere and Ar^+ irradiation, **c)** non-irradiated sample after exposure to a CO_2 atmosphere and **d)** irradiated sample after CO_2 atmosphere exposure, a peak at the binding energy 290 eV is formed (dashed line).

3.4. Chemical reactivity after irradiation

The surface reactivity of the samples has been tested by exposure to CO_2 gas. The surface layer carbon-rich contamination was first removed by heating at 500 °C for 30 min under an O_2 atmosphere. A part of the sample was then irradiated with Ar^+ ions (1 keV) at a flux of 3.6×10^{12} ions cm^{-2} s^{-1} and a fluence of 1.3×10^{16} ions cm^{-2}. The irradiated samples and the non-irradiated sample were then exposed to CO_2 gas at 1 bar for 1 hour at room temperature in the catalytic chamber of the XPS instrument and XPS measurements performed after each step of the experiment (thermal annealing, irradiation and gas exposure).

Figure 9 shows the region of the carbon peak for the main steps of this experiment. Heat treatment with O_2 has removed the main part of the carbon-rich contamination layer. After CO_2 exposure a well developed peak appears at a binding energy 290 eV for the Ar^+-irradiated sample while the non-irradiated one displays a very weak peak at the same binding energy: C 1s/Si 2p ratio is 3 to 5 times higher for the irradiated sample. This peak is characteristic of carbonates (Ardizzone et al. 1997). This experiment thus suggests an elevated chemical reactivity for the irradiated sample.

4. Discussion

One of the main effects measured by XPS after irradiation is a shift of all the peak positions towards lower binding energies. This shift is due to a charging effect, as previously reported by Dukes et al. (1999) for irradiated olivine. It affects all the peaks with the same amplitude, showing that the electron binding energies are not significantly modified by irradiation. Thus the nature of the local environment of the atoms is not fundamentally affected despite the strong processing by irradiation. However, we also observe a progressive broadening of the peaks for all the elements. This could originate from network extension, implying an elongation of the lengths of the Si-O-Si bonds and/or variations in the Si-O-Si dihedral angle. This evolution is frequently found in irradiated materials as studied using XPS (Torrisi et al. 1996; Nesbitt et al. 2004) and is compatible with the progressive amorphization of silicates under irradiation (e.g. Demyk et al. 2001; Carrez et al. 2002; Jäger et al. 2003). XPS peak broadening in silicates would correspond to the broad Si-O stretching and O-Si-O bending vibration bands of silicon-oxygen tetrahedra, SiO_4, in irradiated silicates as observed by infrared spectroscopy.

Our experiments show that the resulting oxidation state of the iron atoms is a function of the flux and of the nature of the ions used in the irradiation experiment. For light ions (H^+ and He^+) and moderated fluxes (below $\sim 4 \times 10^{14}$ ions cm^{-2} s^{-1}) the oxidation of iron can be explained by a direct charge transfer between the incident ion and the iron atoms according to the reaction:

$$Fe^{2+} + He^+(H^+) \Rightarrow Fe^{3+} + He(H). \quad (3)$$

The reduction of iron species is observed for heavy ions (Ar^+) and light ions at high irradiation fluxes (greater than $\sim 4 \times 10^{14}$ ion cm^{-2} s^{-1}). Under these irradiation conditions the energy deposition rate is higher. The resulting high defect production rate probably does not allow the broken atomic bonds to be fully reformed. In this case free oxygen ions can be liberated from broken Fe-O bonds and recombine with other oxygen to form molecular oxygen. This reaction implies electron transfer from the oxygen ions to the iron ions according to the reaction:

$$2Fe^{2+} + 2O^{2-} \Rightarrow 2Fe^0 + O_2. \quad (4)$$

This chemical reaction in irradiated oxides is not surprising and has been already deduced from electron irradiation experiments (e.g. Davoisne & Leroux 2006). The formation of molecular oxygen could contribute to the bubble formation observed in irradiated samples (Demyk et al. 2001; Carrez et al. 2002). Iron reduction has already been deduced from the ion-irradiation of iron oxides (Pirlot et al. 2001) and silicates (Yin et al. 1975; Dukes et al. 1999; Carrez et al. 2002).

Studying the different core levels could help to localise the depth of the irradiation induced damage or the chemical modification of the surface. According to the binding energies, the mean free path for Mg 1s and Mg 2p are 1 and 5 nm, respectively. During irradiation we have shown that the Mg 1s/Si 2p ratio increases more than the Mg 2p/Si 2p ratio. This effect is not due to preferential sputtering of Si since the Mg 2p/Si 2p and the Fe 2p/Si 2p are still relatively constant. This differential evolution is better explained by magnesium segregation at the sample surface resulting from charge trapping due to ion implantation during irradiation. The implantation of positive charge inside the olivine can generate an electric field. In olivine the cations Mg^{2+} and Fe^{2+} are in octahedral sites and are more mobile than the silicon, which is in SiO_4 tetrahedra. The ions could therefore diffuse to the surface due to the presence of the electric field. Under irradiation the migration of species and surface composition modification assisted by an electric field has been already

observed, in particular, for insulators in which the charge effect appeared rapidly (e.g. Battaglin et al. 1982; Mosbah & Duraud 1998; Zemek & Gedeon 2004).

Our results show that the irradiated surfaces are strongly modified during ion irradiation. The main trend is the formation of surface corrugations. This evolution is well-known and includes two competing mechanisms, i.e., the process of erosion due to sputtering and the process of surface diffusion which tend to smooth the features created by the ion impacts. The wavelengths and amplitudes of the observed hillocks are a function of the energy of the incident ions, as shown by the He irradiation experiments performed at 1 and 4 keV. The size of the hillock domains are typically 50 nm for a 4 keV He^+ irradiation but only 20 nm for 1 keV He^+ irradiation. This difference is probably related to the nature of the interaction that takes place during irradiation. At low energy, the nuclear interactions are predominant while at higher energy the electronic interactions become dominant, but, more importantly, the implantation depth at 1 keV is only ∼10 nm, i.e., the extreme surface is highly processed by the nuclear interactions that then prevent significant growth of the hillocks. At 4 keV the implantation depth is ∼30 nm and the atoms at the surface are mainly subjected to electronic interactions, which favor atomic mobility and the growth of hillocks. The AFM images also showed elongated hillocks at the periphery of the irradiated areas. This is probably an effect of the surface charging due to ion implantation that then deflects the incident ion beam radially with respect to the irradiation center. The anisotropy clearly shows that the incident ions interacted with the surface at inclined angles. It is interesting to note that the domain size of elongated hillocks is found to decrease with increasing distance from the center of the irradiated zone. Under these conditions the ion implantation depth is lower as the inclination angle increases and this thus favors the nuclear interactions close to the surface. Finally, the AFM study showed that surface morphology after irradiation is not stable with time. The post-irradiation modification can result from a relaxation of the surface after irradiation and/or from interaction between air and the irradiated surface. These observations suggest that the irradiated surfaces are chemically highly reactive.

The highly reactive behavior of the irradiated samples is also highlighted by the CO_2 exposure experiment. The irradiated surfaces clearly favor the reaction of the surface with CO_2 leading to the formation of magnesium carbonate $MgCO_3$. Indeed, the surface reactivity of the enriched MgO surface has a basic chemical character. Such a surface easily reacts with CO_2 which has an acidic chemical character. We propose the following reaction:

$$MgO(surf) + CO_2(gas) \Rightarrow MgCO_3(surf). \quad (5)$$

The formation of carbonates after gas-grain irradiation has already been seen in the experiments of Toppani et al. (2005). Our experiments show that chemical reactions can be enhanced by irradiation surface processing. All modifications (morphological and chemical) which can affect the grain surface can influence the nature and the kinetics of the catalytic processes. We have observed silicate surface morphological modification during ion irradiation, which leads to the appearance of particular features (hillocks, oriented anisotropic structure) and an increase in the surface roughness. Irradiation also produces atomic defects at the surface, not observable by our analytical investigation tools. This evolution increases the surface specific area and modifies the surface energy and thus leads to favourable conditions for chemical reactions or catalysis at the grain surface.

5. Conclusion and astrophysical implications

The amorphisation of silicate minerals by ion irradiation (gas-grain collisions) in supernovae-generated shockwaves in the interstellar medium has been successfully reproduced in laboratory experiments involving the low-energy ion irradiation of silicates (Demyk et al. 2001, 2004; Carrez et al. 2002; Schrempel et al. 2002; Jäger et al. 2003; Brucato et al. 2004). However, little is currently known about the chemical evolution effects under ion irradiation. Our experiments suggest that the chemical changes we observed are driven by the electric field, which accompanies the experimental ion irradiation. This electric field effect probably does not occur during the ion irradiation of grains in supernova shocks in the ISM because the implantation is into negatively charged grains and any implanted charge will be neutralised. The negative grain charge in shocks arises from the high electron thermal velocity (with respect to the ions) and therefore a higher electron sticking rate onto the grains. In the diffuse ISM, where the grains are predominantly positively charged, ion irradiation occurs via a very low flux but very high energy cosmic rays. Our experimental results are, however, not applicable to such high energy cosmic ray irradiation. Thus, the charging effect that we find here is probably not generally applicable to interstellar grains and is a characteristic of our experimental conditions, i.e., the positive ion irradiation of an insulator. Despite this lack of immediate application to the astrophysical situation, we think that irradiation/charging effects could perhaps have long-term effects for the catalytic properties of interstellar grains and should be taken into account. For example, if the changes in the silicate surface composition and structure induced by irradiation (e.g., surface roughness and/or bulk porosity) are long-lasting, they could lead to an enhanced formation rate for surface-catalysed molecular hydrogen formation and might also influence the initial stages of ice mantle accretion in molecular clouds, i.e., an enhanced surface area for the initial accretion of gas phase species. Both of these effects would be the result of an increased grain surface-to-volume ratio in rough-surfaced, porous, previously-irradiated grains. This hypothesis is supported by our surface reactivity experiments, which show enhanced reaction with gas phase CO_2 leading to surface magnesium carbonate formation. Carbonates have been observed recently in protostars (Ceccarelli et al. 2002; Chiavassa et al. 2002) and in the dust shells around evolved stars (Kemper et al. 2002).

Our results may also have some implications for the evolution of interstellar silicates because we note that the dust-forming elemental depletions and their environment-dependent distribution in the ISM are difficult to explain by irradiation mechanisms only, e.g., the unexpected volatility of silicon in the ISM, with respect to magnesium and iron, that does not follow the expected elemental sputtering trends (Tielens 1998; Jones 2004). The grain charge could play a role, as shown by the athermal magnesium segregation on surfaces during our experiments. However, extrapolation to ISM conditions is not obvious since the irradiation flux strongly differs from experiments. At low flux, charge relaxation will be more efficient.

Another modification that we have observed during ion irradiation is the change in the iron oxidation state. We have shown that the iron valence state depends on the irradiation flux. For fluxes less than 4×10^{14} ions cm^{-2} s^{-1} iron oxidation is predominant and is interpreted as a charge transfer between the incident ion and the iron in the silicate. In supernovae shockwaves the flux is estimated to be only 10^7 ions cm^{-2} s^{-1} (Jones et al. 1996), conditions that would seem to be favorable for iron oxidation rather than reduction.

References

Ardizzone, S., Bianchi, C. L., Fadoni, M., & Vercelli, B. 1997, Appl. Surf. Sci., 236, 661

Battaglin, G., Mea, G. D., Marchi, G. D., et al. 1982, J. Phys. C: Solid State Phys., 15, 5623

Bradley, J. P. 1994, Science, 265, 925

Brucato, J. R., Strazzulla, G., Baratta, G., & Colangeli, L. 2004, A&A, 413, 395

Carrez, P., Demyk, K., Cordier, P., et al. 2002, Meteoritics Planet. Sci., 37, 1599

Ceccarelli, C., Caux, E., Tielens, A. G. G. M., et al. 2002, A&A, 395, L29

Chiavassa, A., Ceccarelli, C., Tielens, A. G. G. M., Caux, E., & Maret, S. 2002, A&A, 432, 547

Davoisne, C., & Leroux, H. 2006, NIMB, 243, 371

Demyk, K., Dartois, E., Wiesemeyer, H., Jones, A. P., & d'Hendecourt, L. 2000, A&A, 364, 170

Demyk, K., Carrez, P., Leroux, H., et al. 2001, A&A, 368, L38

Demyk, K., d'Hendecourt, L., Leroux, H., Jones, A. P., & Borg, J. 2004, A&A, 420, 233

Dukes, C. A., Baragiola, R. A., & McFadden, L. A. 1999, J. Geophys. Res., 104, 1865

Ellison, D. C., Drury, L. O. C., & Meyer, J. P. 1997, ApJ, 487, 197

Graat, P. C. J., & Somers, M. A. J. 1996, Appl. Surf. Sci., 100, 36

Grimblot, J. 1995, L'analyse de surface des solides, ed. Masson, France

Guittet, M. J., Crocombette, J. P., & Gautier-Soyer, M. 2001, Phys. Rev. B, 63, 125117

Hochella, M. F. J. 1988, Rev. Mineral. Geophys., 18, 573

Jäger, C., Molster, F. J., Dorschner, J., et al. 1998, A&A, 339, 904

Jäger, C., Fabian, D., Schrempel, F., et al. 2003, A&A, 401, 57

Jones, A. P. 2000, J. Geophys. Res., 105, 10257

Jones, A. P. 2004, in Astrophysics of dust, ed. A. N. Witt, G. C. Clayton, & B. T. Draine, ASP Conf. Ser., 309, 347

Jones, A. P., Tielens, A. G. G. M., Hollenbach, D. J., & Kee, C. F. M. 1994, ApJ, 433, 797

Jones, A. P., Tielens, A. G. G. M., & Hollenbach, D. J. 1996, ApJ, 469, 740

Kemper, F., Jäger, C., Waters, L. B. F. M., et al. 2002, Nature, 415, 295

Kemper, F., Vriend, W. J., & Tielens, A. G. G. M. 2004, ApJ, 609, 826

Kemper, F., Vriend, W. J., & Tielens, A. G. G. M. 2005, ApJ, 633, 534

Molster, F. J., Waters, L. B. F. M., & Tielens, A. G. G. M. 2002a, A&A, 382, 222

Molster, F. J., Waters, L. B. F. M., Tielens, A. G. G. M., Koike, C., & Chihara, H. 2002b, A&A, 382, 241

Mosbah, M., & Duraud, J. P. 1998, NIMB, 141, 594

Nesbitt, H. W., Bancroft, G. M., Davidsob, R., McIntyre, N. S., & Pratt, A. R. 2004, Amer. Mineral., 89, 878

Pirlot, C., Deniau, G., Viel, P., et al. 2001, NIMB, 185, 71

Schott, J., & Berner, R. A. 1983, Geochim. Cosmochim. Acta, 47, 2233

Schrempel, F., Jäger, C., Fabian, D., et al. 2002, NIMB, 191, 411

Scofield, J. H. 1976, J. Electron. Spectrosc. Rel. Phenomena, 8, 129

Seyama, H., & Soma, M. 1985, J. Chem. Soc. Faraday Trans., 1, 81, 485

Shirley, D. A. 1972, Phys. Rev. B, 5, 4709

Sylvester, R. J., Kemper, F., Barlow, M. J., et al. 1999, A&A, 352, 587

Tamuna, S., Powell, C. J., & Penn, D. R. 1993, Surf. Interface Anal., 20, 77

Tielens, A. G. G. M. 1998, ApJ, 499, 267

Tielens, A. G. G. M., Kee, C. F. M., Seab, C. G., & Hollenbach, D. J. 1994, ApJ, 431, 321

Toppani, A., Robert, F., Libourel, G., et al. 2005, Nature, 437, 1121

Torrisi, A., Licciardello, A., Ancarani, V., Massimiliano, C., & Puglisi, O. 1996, NIMB, 116, 342

Wagner, C. D., Davis, L. E., & Riggs, W. M. 1980, Surf. Interface Anal., 2, 53

Waters, L. B. F. M., Molster, F. J., de Jong, T., et al. 1996, A&A, 315, L361

Yin, L. I., Tsang, T., & Adler, I. 1975, Geophys. Res. Lett., 2, 33

Zemek, J., & Gedeon, O. 2004, J. Non-Cryst. Solids, 337, 268